APL Materials

Refractory metal-based ohmic contacts on β-Ga_2O_3 using TiW

Cite as: APL Mater. **10**, 071108 (2022); https://doi.org/10.1063/5.0094661
Submitted: 05 April 2022 • Accepted: 20 June 2022 • Published Online: 12 July 2022

Kornelius Tetzner, Robert Schewski, Andreas Popp, et al.

Refractory metal-based ohmic contacts on β-Ga_2O_3 using TiW

Cite as: APL Mater. 10, 071108 (2022); doi: 10.1063/5.0094661
Submitted: 5 April 2022 • Accepted: 20 June 2022 •
Published Online: 12 July 2022

Kornelius Tetzner,[1,a] Robert Schewski,[2] Andreas Popp,[2] Saud Bin Anooz,[2] Ta-Shun Chou,[2] Ina Ostermay,[1] Holm Kirmse[3] and Joachim Würfl[1]

AFFILIATIONS

[1] Ferdinand-Braun-Institut, Leibniz-Institut für Höchstfrequenztechnik, Gustav-Kirchhoff-Straße 4, 12489 Berlin, Germany
[2] Leibniz-Institut für Kristallzüchtung (IKZ), Max-Born-Straße 2, 12489 Berlin, Germany
[3] Institut für Physik, Humboldt-Universität zu Berlin, Newtonstr. 15, 12489 Berlin, Germany

[a] **Author to whom correspondence should be addressed:** kornelius.tetzner@fbh-berlin.de

ABSTRACT

The present work investigates the use of the refractory metal alloy TiW as a possible candidate for the realization of ohmic contacts to the ultrawide bandgap semiconductor β-Ga_2O_3. Ohmic contact properties were analyzed by transfer length measurements of TiW contacts annealed at temperatures between 400 and 900 °C. Optimum contact properties with a contact resistance down to 1.5×10^{-5} Ω cm^2 were achieved after annealing at 700 °C in nitrogen on highly doped β-Ga_2O_3. However, a significant contact resistance increase was observed at annealing temperatures above 700 °C. Cross-sectional analyses of the contacts using scanning transmission electron microscopy revealed the formation of a TiO_x interfacial layer of 3–5 nm between TiW and β-Ga_2O_3. This interlayer features an amorphous structure and most probably possesses a high amount of vacancies and/or Ga impurities supporting charge carrier injection. Upon annealing at temperatures of 900 °C, the interlayer increases in thickness up to 15 nm, featuring crystalline-like properties, suggesting the formation of rutile TiO_2. Although severe morphological changes at higher annealing temperatures were also verified by atomic force microscopy, the root cause for the contact resistance increase is attributed to the structural changes in thickness and crystallinity of the interfacial layer.

The recent developments in the fabrication of electronic devices based on the semiconductor β-Ga_2O_3 have demonstrated the high potential of this material to be used in next-generation power electronics applications.[1–3] Due to the ultra-wide bandgap of 4.8 eV, a high breakdown strength of 8 MV/cm is expected, which could pave the way for power devices with even higher breakdown voltages and efficiencies than are possible with the SiC and GaN counterparts.[4,5] Current research activities using β-Ga_2O_3 are preferentially focusing on the development of Schottky barrier diodes[6–8] and field-effect transistors.[9–13] Promising performances have been achieved so far with electronic devices reaching a peak field strength as high as 5.5 MV/cm[14] and breakdown voltages up to 8.03 kV.[15] Apart from the expected high breakdown strength, β-Ga_2O_3, like any other wide bandgap semiconducting material, offers the possibility to be used in high-temperature electronic applications, such as in the field of automotive or aerospace engineering.[16–18] However, the predominately used ohmic contact system Ti/Au for β-Ga_2O_3, which is commonly annealed around 500 °C for contact formation, shows severe degradation when exposed to temperatures beyond 500 °C.[19,20] To overcome this issue, this paper analyzes the ohmic contact properties of the refractory metal alloy TiW (10:90 wt. %) on β-Ga_2O_3 for potential high-temperature applications. Although it has recently been shown that pure tungsten forms Schottky contacts to β-Ga_2O_3,[21,22] we demonstrate that by the addition of 10% titanium, reliable ohmic contacts to β-Ga_2O_3 can be realized. Optimum contact formation is achieved at annealing temperatures of 700 °C, emphasizing the high-temperature stability of this metallization system. However, significant degradation is identified beyond this temperature due to changes in the TiW/β-Ga_2O_3 interface quality.

In order to analyze the impact of the doping concentration of the semiconducting β-Ga_2O_3 on the contact resistance, two types of structures, named structure A and structure B, were fabricated,

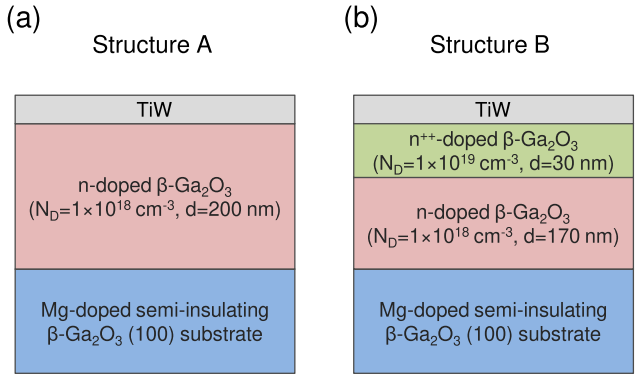

FIG. 1. Schematic structure of the fabricated β-Ga_2O_3 samples showing structure A featuring a uniformly n-doped MOCVD layer with a doping concentration of 1×10^{18} cm^{-3} (a) and structure B featuring an additional heavily n^{++}-doped layer with a doping concentration of 1×10^{19} cm^{-3} atop (b) for cross-comparison of the contact resistances of TiW.

as shown in Fig. 1. For both structures, the experiments started with the homoepitaxial growth of a Si-doped semiconducting β-Ga_2O_3 layer by metal organic chemical vapor deposition (MOCVD) on Mg-doped semi-insulating β-Ga_2O_3 (100) substrates.[23,24] The substrates with dimensions of $10 \times 10 \times 0.5$ mm^3 were prepared with a miscut of 4° from 2 in. diameter bulk β-Ga_2O_3 single crystals obtained by the Czochralski method at the Leibniz-Institute for Crystal Growth.[25–27] Triethylgallium (TEGa) was used as the gallium precursor, pure O_2 as the oxygen source, tetraethyl-orthosilicate (TEOS) as the Si-dopant, and high purity Ar as the carrier gas. A growth temperature of 825 °C and a chamber pressure of 25 mbar were used, which resulted in a growth rate of about 3.6 nm/min. The molar flows of the used gases were adjusted to realize epitaxial Ga_2O_3 layers with a doping concentration N_D of around 1×10^{18} cm^{-3} and a charge carrier mobility μ of 106 cm^2/Vs for both structure types. In addition to this layer, a 30 nm thin heavily doped n^{++}-layer with a doping concentration of around 1×10^{19} cm^{-3} and a charge carrier mobility of 33 cm^2/Vs was deposited subsequently atop in the case of structure B. The total thickness of the epitaxial layers for both structure types was set to 200 nm. Doping concentration and mobility values of the respective epitaxial layers were determined separately for each epitaxial layer by Hall measurements on reference test samples.

For the electrical characterization of the TiW ohmic contacts, circular transfer length measurement (TLM) structures were fabricated by starting with a surface preparation of the β-Ga_2O_3 samples in BCl_3-Ar-plasma. Here, the samples were transferred into a reactive ion etch (RIE) system in order to etch ~10 nm of Ga_2O_3 within the ohmic contact region. Previously, it has been reported that a short RIE treatment of Ga_2O_3 prior to the metal contact deposition leads to the generation of high-density surface defects, such as oxygen vacancies that act as donors enhancing the charge carrier injection.[28,29] Subsequently, TiW contacts with a thickness of 150 nm were deposited by an RF-sputter process in a Leybold Z590 using a Ti:W (10:90 wt. %) target with 99.99% purity. The sputtering process was performed at an RF power of 160 W, an Ar-flow of 15 sscm, and a chamber pressure of 0.5 Pa. Afterward, the metal layer was structured using photolithography and SF_6-based dry etch processing. The circular TLM structures featured a pad diameter of 200 μm and electrode spacings of 4, 8, 12, 16, 20, and 24 μm. Finally, the samples were subjected to rapid thermal annealing for 60 s in a nitrogen atmosphere at temperatures ranging from 400 to 900 °C.

Sheet and contact resistances were extracted from the TLM structures at room temperature using the four-point probe method with measuring currents between −100 and 100 mA. The surface topography of the as-deposited and annealed TiW layers was investigated by atomic force microscopy (AFM) in tapping mode using a Bruker Dimension Edge AFM system. Scanning Transmission Electron Microscope [(S)TEM] investigations were performed with a FEI Titan 80-300 transmission microscope operated at an acceleration voltage of 300 kV. The microscope is equipped with a high brilliance X-FEG emitter and a CS corrector for imaging. Energy-dispersive x-ray spectroscopy (EDX) measurements were performed using a JEOL JEM2200FS operated at an acceleration voltage of 200 kV. TEM samples were prepared in cross-sectional geometry by conventional plan parallel polishing down to a thickness of about 5 μm. For achieving electron transparency, the samples were further thinned by ion-milling in a Gatan PIPS, with an acceleration voltage of 3.5 kV. As a cleaning step, the acceleration voltage was stepwise reduced down to 0.2 kV.

Figure 2 shows the I–V measurements of circular TLM patterns with an electrode spacing of 4 μm for structures A and B, which were annealed at different temperatures. It can be seen that structure A shows significant non-ohmic properties for all annealing temperatures with non-linear curve progressions. A similar trend can be observed for samples based on structure B, which have been annealed at temperatures below 700 °C. However, a distinct linear correlation between current and voltage is observed at an annealing temperature of 700 °C, emphasizing ohmic contact properties, which disappears again at annealing temperatures above 700 °C. In order to extract the values for the contact resistance R_C and the specific contact resistivity ρ_C of the TiW on β-Ga_2O_3 for all the annealed samples based on structures A and B, the total resistance as a function of the electrode spacing is plotted. It should be noted that the extraction of the contact resistance for all curves was done at low voltages where the curves still show almost linear behavior, avoiding underestimation of the resistance values. Although the TLM method is usually only applied to contacts that show full ohmic properties, this approach allowed a qualitative comparison of the

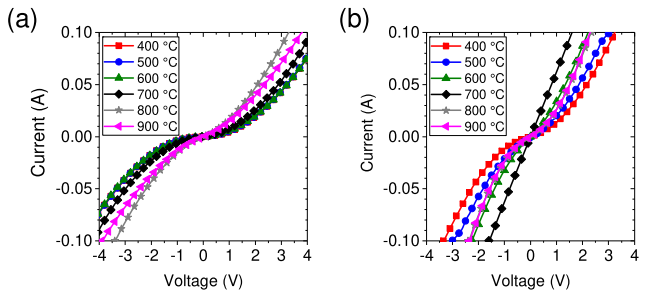

FIG. 2. Representative I–V characteristics of a TLM pattern with an electrode spacing of 4 μm on structure A (a) and structure B (b) measured after annealing at different temperatures.

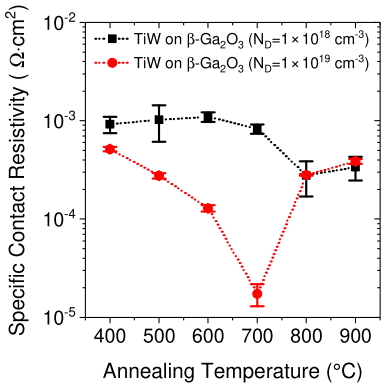

FIG. 3. Comparison of the specific contact resistivity of structures A and B as a function of the annealing temperature.

contact properties of the TiW contacts annealed at different temperatures. A comparison of the specific contact resistivity as a function of the annealing temperature for both structures is shown in Fig. 3. Here, it can be seen that in the case of structure A, the value for ρ_C stays almost constant at around 10^{-3} Ω cm^2 for annealing temperatures between 400 and 700 °C and slightly goes down to around 2×10^{-4} Ω cm^2 after annealing above 700 °C. The latter value equals a contact resistance of 8 Ω mm for each contact, which is unacceptably high for use in efficient electronic devices, since it already contributes a high percentage of the total on-resistance of recent β-Ga_2O_3 power transistors.[12,13] Structure B, in turn, shows a steady decrease in the specific contact resistivity with increasing annealing temperature and reaches a minimum value of 1.5×10^{-5} Ω cm^2 at 700 °C. However, at higher annealing temperatures above 700 °C, the contact resistivity increases again to values similar to those of structure A. The TLM plot of structure B, which was annealed at 700 °C, showing the lowest specific contact resistivity, is presented in Fig. 4, revealing a contact resistance of 1.6 Ω mm for each contact. In addition to R_C and ρ_C, the TLM plot also allows us to extract the sheet resistance R_S, which did not change with the annealing temperature for both structures and had a value of 2.2 and 1.6 kΩ/sq for structures A and B, respectively. As shown in the previously reported investigations, the optimum specific contact resistance of Ti/Au contacts to β-Ga_2O_3 is typically in the range of 10^{-6} to 10^{-5} Ω cm^2, which is usually achieved by highly n-type doping of the β-Ga_2O_3 contact region prior to metal deposition either using Si-implantation[12,30,31] or epitaxial regrowth.[14,32] Up to now, the lowest contact resistance on β-Ga_2O_3 with a value of 8.3×10^{-7} Ω cm^2 was achieved by using the latter approach.[36] Benchmarking our optimum contact resistance value with the data from the literature emphasizes the good ohmic contact properties of TiW to β-Ga_2O_3 annealed at 700 °C.

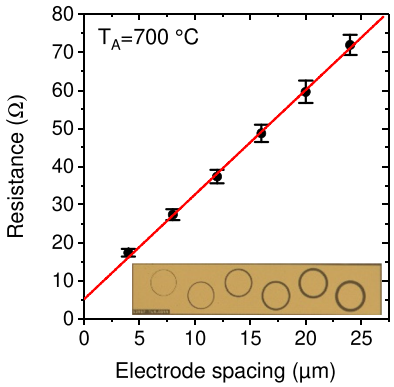

FIG. 4. TLM plot showing the fitted curve of the total resistance as a function of the electrode spacing for structure B annealed at 700 °C. The inset shows the TLM pattern used for the experiments.

In order to investigate the impact of the annealing temperature on the surface morphology of the sputtered TiW on the β-Ga_2O_3 epitaxial substrates, AFM measurements were carried out on samples with as-deposited TiW layers as well as on samples annealed at 700 and 900 °C. The results of these measurements are presented in Fig. 5 and indicate smooth TiW layers right after deposition with a root-mean-square (rms) roughness of 0.8 nm, which is only slightly higher than the rms roughness value of the β-Ga_2O_3 epitaxial layer of 0.2 nm. After annealing at 700 °C, the surface roughness slightly increases to an rms value of 1.7 nm, which still indicates smooth surfaces of the TiW. However, annealing at 900 °C results in the formation of layers with increased surface roughness up to an rms roughness value of 3.6 nm. The height distribution presented in Fig. 5(d) illustrates these observations, showing a two-times higher rms roughness for samples annealed at 700 °C as well as a four-times higher rms roughness for samples annealed at 900 °C compared to

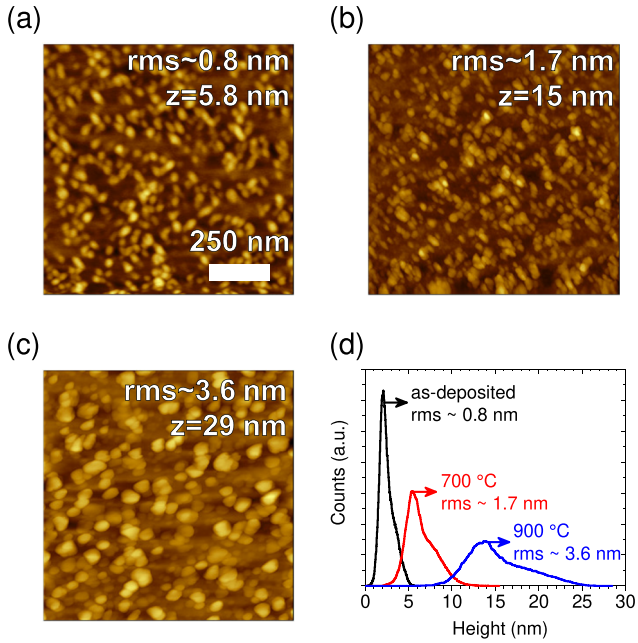

FIG. 5. AFM measurements of sputtered TiW on β-Ga_2O_3 as-deposited (a) after RTA at 700 °C (b) and 900 °C in N_2 atmosphere (c) as well as the corresponding height distributions (d).

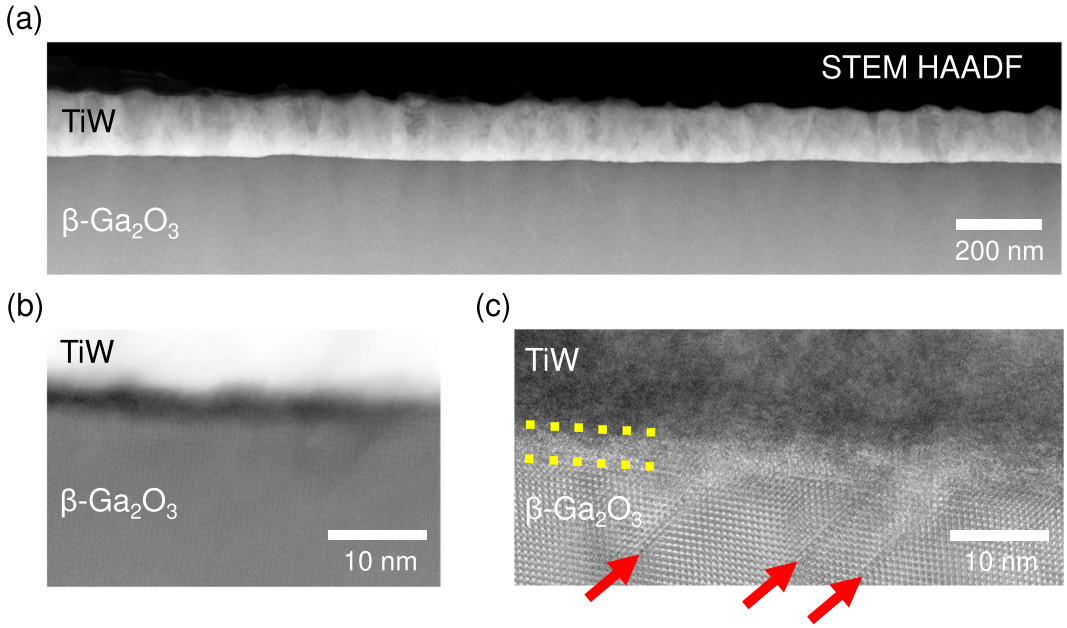

FIG. 6. STEM HAADF images of the interface region between TiW and β-Ga_2O_3 annealed at 700 °C for 60 s in low (a) and high magnification (b) as well as a high-resolution TEM image (c), revealing defects along the $(\bar{2}01)$ lattice planes (red arrows).

the as-deposited layers. In addition, the deteriorated surface morphology at the higher annealing temperature is reflected by a distinct broadening of the height distribution. This significant change in the surface morphology between 700 and 900 °C could be an indicator that the interface quality between the TiW and the β-Ga_2O_3 is reduced, explaining the observed increase in the specific contact resistivity for structure B. In order to verify this assumption, cross-sections of structure B annealed at 700 °C and 900 °C were prepared and analyzed using TEM.

Figure 6(a) shows a low magnification STEM HAADF image of the contact structure of the 700 °C annealed sample in the cross-sectional view. The TiW is much brighter in comparison to the β-Ga_2O_3 layer, caused by the higher mean atomic number of the TiW compared to the β-Ga_2O_3. The surface structure of the metal contact is in good agreement with the AFM images shown in Fig. 5. Although the interface between the contact metal and the β-Ga_2O_3 layer appears to be completely sharp in this image, a small interlayer [Figs. 6(b) and 6(c)] with a thickness of about 3–5 nm can be observed at higher magnification. This interlayer appears dark in the STEM HAADF image [Fig. 6(b)] in contrast to the β-Ga_2O_3 layer as well as to the TiW contact, while no atomic pattern can be resolved. A similar interlayer has been previously described by Peterson *et al.* in the case of Ti/Au contacts, indicating the formation of a TiO_x interlayer.[33,34] To elaborate the atomic species involved in the formation of this interlayer, we performed STEM EDX measurements, as shown in Fig. 7. The STEM HAADF image shows the interface region between the TiW and the β-Ga_2O_3 layer of the 700 °C annealed sample. Figures 7(b)–7(e) represent the corresponding elemental distribution maps of this area as measured by STEM EDX. We included the main species in the specimen, namely, oxygen, tungsten, titanium, and gallium. The K_α line was chosen for the detection of oxygen, titanium, and gallium, while the L_α line

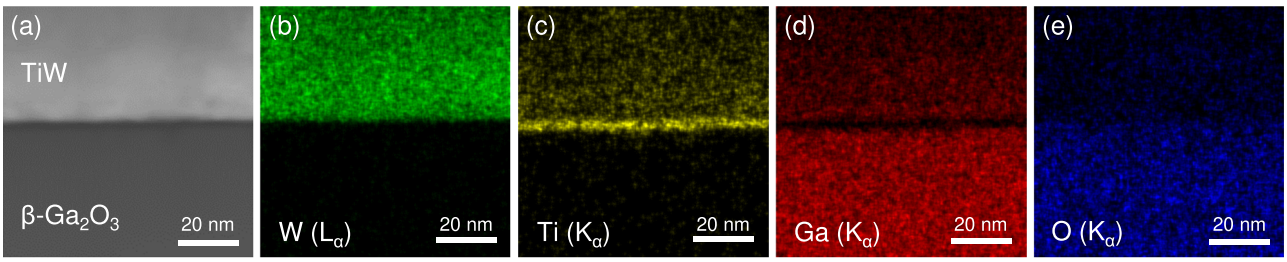

FIG. 7. STEM HAADF image of the interface region between TiW and β-Ga_2O_3 annealed at 700 °C for 1 min (a) and respective EDX maps of tungsten, titanium, gallium, and oxygen [(b)–(e)].

was used for tungsten since the W-K line is far above the maximum energy of the EDX spectrum of 20 keV. First of all, it can be seen that the tungsten signal can only be detected in the contact region, indicating a high stability of tungsten. Another observation is that gallium can be found in the β-Ga_2O_3 layer as well as in the TiW contact. This is due to an out-diffusion of Ga atoms as previously described.[33] Interestingly, almost no Ga signal can be detected in the interface region (dark area in the STEM HAADF image), whereas oxygen can be partially found here as well as in the β-Ga_2O_3 layer. The strongest signal in the interface region is generated by titanium. This indicates that the intermediate phase is most likely based on TiO_x with very low gallium concentration as is also the case with Ti/Au contacts on β-Ga_2O_3. However, it should be noted that the formation of this interlayer with comparable dimensions using Ti/Au contacts was already observed at an annealing temperature of 470 °C.[33,34] Since titanium is randomly distributed within the TiW layer with a concentration of only 10 wt. %, we suspect that the limited availability of titanium at the TiW/β-Ga_2O_3 interface is the reason that higher temperatures are necessary to form a TiO_x interlayer with a comparable thickness. Another feature can be observed in the high-resolution TEM image [Fig. 6(c)] below this interlayer in the β-Ga_2O_3 layer. Line shape contrasts at the interface are appearing along the $(\bar{2}01)$ lattice planes (marked by arrows). These defects are not present in as-grown homoepitaxial layers and are most likely formed due to a diffusion process of either Ga or O from the β-Ga_2O_3 layer into this interlayer. Moreover, EDX analysis indicates the diffusion of Ti downward into these defective regions forming TiO_x. This means that even at annealing temperatures of 700 °C, we observe the solid solution reaction of the present species, which has been also observed previously.[35]

Figure 8(a) shows a low magnification STEM HAADF image of the interface of a β-Ga_2O_3 sample coated with TiW and annealed at 900 °C. One of the first noticeable features in contrast to the sample annealed at 700 °C is the formation of metal islands on top of the TiW contact layer, which is in good agreement with the rough surface observed by AFM. The second noticeable feature is a much more pronounced, dark but discontinuous line at the interface between the β-Ga_2O_3 and the TiW contact as compared to the sample annealed at 700 °C. High-resolution STEM HAADF images taken at different positions of this interface region are presented in Figs. 8(b) and 8(c), verifying an increase of the interlayer thickness up to 5–15 nm. In addition, the layer exhibits increased structural ordering. Figure 8(b) reveals a quadratic pattern of the projected atomic columns with an inter-atomic distance (white lines) of 0.32 nm. In contrast to this, only bright lines are seen in Fig. 8(c) with no sign of distinct atomic columns, indicating an orientation of the crystalline material, where the interatomic distance within the lines is smaller than the resolution limit of the imaging method. The distance between the white lines is again about 0.32 nm. These observations most likely correspond to an intermixed, polycrystalline, tetragonal, or cubic phase, forming rotational domains with respect to the β-Ga_2O_3 layer.

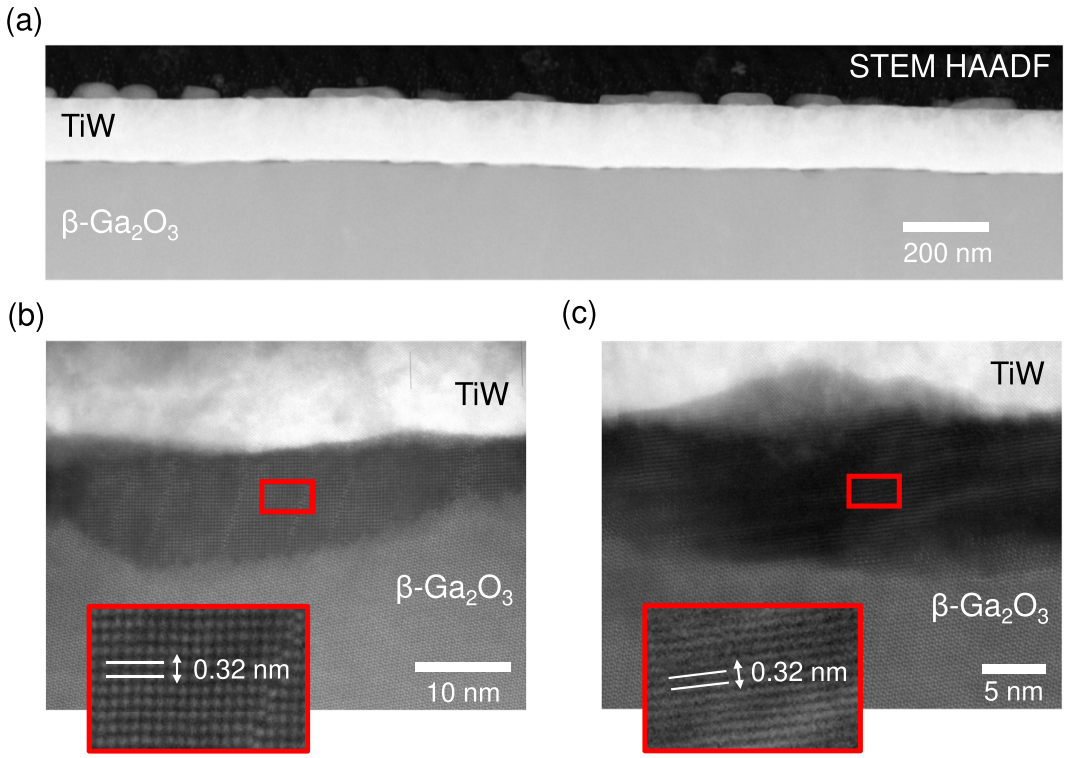

FIG. 8. STEM HAADF images of the interface region between TiW and β-Ga_2O_3 annealed at 900 °C for 60 s in low (a) and high resolution [(b) and (c)]. The high-resolution images were taken at different positions of the interlayer, revealing its crystalline structure with different orientations and a lattice plane distance of 0.32 nm.

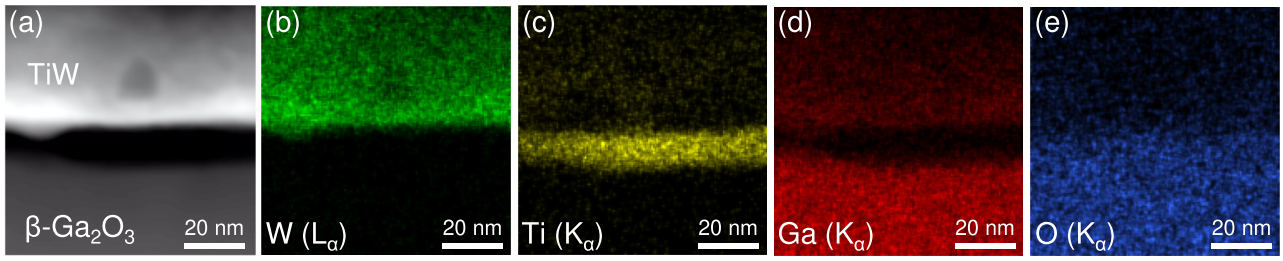

FIG. 9. STEM HAADF image of the interface region between TiW and β-Ga_2O_3 annealed at 900 °C for 1 min (a) and respective EDX maps of tungsten, titanium, gallium, and oxygen [(b)–(e)].

We also performed STEM EDX measurements on this sample, as shown in Fig. 9, with a STEM HAADF image showing the interface region between the TiW and the β-Ga_2O_3 layer as well as the corresponding elemental distribution maps of this area. The analysis reveals that the elemental distribution is almost identical to the sample annealed at 700 °C with the exception of a thicker interface region. Again, this region mostly consists of titanium and oxygen, indicating a titanium oxide intermediate phase. The main crystal modifications of titanium oxide are anatase (tetragonal), brookite (orthorhombic), and rutile (tetragonal). A comparison of these modifications with the experimental findings excludes anatase and brookite. The pattern observed in the high-resolution HAADF STEM images of Fig. 8(b) perfectly agrees with the rutile structure seen along the ⟨001⟩ projection. In addition, the measured lattice distances of 0.32 nm are in perfect agreement to the {110} planes of pure TiO_2 in the rutile modification.

Based on the analyses and observations carried out in this study, we can draw the following conclusions. At annealing temperatures of 700 °C, an interdiffusion process of Ti from the TiW contact into the β-Ga_2O_3 layer takes place. Here, Ti starts to react and steals oxygen from β-Ga_2O_3 by partially substituting Ga atoms as has been previously observed with Ti/Au contacts on β-Ga_2O_3 at annealing temperatures of 470 °C.[33] The substituted Ga, in turn, starts to diffuse upward into the TiW contact. The 3–5 nm thin TiO_x layer features amorphous properties and most probably possesses a high amount of vacancies and/or Ga impurities, which improves charge carrier injection from the TiW contact into β-Ga_2O_3, resulting in a low contact resistance. At higher annealing temperatures beyond 700 °C, this TiO_x interlayer dramatically alters its properties. First, the thickness increases up to 15 nm, and second, the crystallographic structure changes from an amorphous to a polycrystalline state of tetragonal TiO_2 (rutile). In this regard, we can assume that the amount of electrically active impurities in this interlayer is significantly reduced, which in combination with the increased thickness leads to a higher contact resistance. Furthermore, it can be stated that a stable ohmic contact based on TiW can only be realized on highly doped n^{++} β-Ga_2O_3 layers with doping concentrations of $\geq 1 \times 10^{19}$ cm^{-3}. In contrast to pure Ti/Au contacts to Ga_2O_3, we believe that a much higher annealing temperature of 700 °C is needed for the TiO_x interlayer formation in case of pure TiW contacts. Since the amount of titanium within the TiW alloy is relatively low and, thus, the availability of titanium at the TiW/β-Ga_2O_3 interface is limited, we suspect that higher temperatures are necessary to support titanium diffusion toward this interface, resulting in a sufficient accumulation for the TiO_x interlayer formation.

In conclusion, this work demonstrates the possibility of realizing ohmic contacts based on TiW on β-Ga_2O_3. Despite the known fact that pure W only forms Schottky contacts with β-Ga_2O_3, we were able to achieve low contact resistances down to 1.5×10^{-5} Ω cm^2 by the addition of 10% Ti. This emphasizes that Ti plays a dominant role in the contact formation. A high annealing temperature of 700 °C is needed in order to initiate the diffusion process of Ti toward the TiW/β-Ga_2O_3 interface where it starts to react with O, leading to the formation of a thin amorphous TiO_x interface layer. We suspect that existing vacancies, defect states, or Ga impurities in this interlayer improve the charge carrier transport mechanism, leading to the reduction of contact resistance. Upon annealing at higher temperatures, the contact resistance increases due to the increase of the interlayer thickness and a modification of the structural properties. The as-formed rutile TiO_2 features a lower defect density as well as a low concentration of Ga impurities, which hinders the charge carrier injection. The investigations prove that an ohmic contact to β-Ga_2O_3 can be realized using TiW, which is stable up to temperatures of 700 °C. This is more than 200 °C higher than is possible with the conventionally used Ti/Au metallization. Nevertheless, it should be noted that highly doped β-Ga_2O_3 is a mandatory requirement to achieve this.

The authors thank Z. Galazka from IKZ for providing β-Ga_2O_3 wafers for homoepitaxy. Furthermore, the authors would like to thank the colleagues in the process department at FBH for process technological support, in particular, A. Arnlind for AFM measurements as well as N. Thiele for RTA processing. H. Lawrenz from FBH is acknowledged for the image preparation of the EDX data. This work was performed in the framework of GraFOx, a Leibniz-Science Campus partially funded by the Leibniz Association. Furthermore, this work was funded by the Federal Ministry of Education and Research in Germany within the frame of the Joint Research Project OXIKON (Funding No. 03VP03711) as well as within the Research Project GoNext (Funding No. 16 ES1084K).

AUTHOR DECLARATIONS

Conflict of Interest

The authors have no conflicts of interest to disclose.

Author Contributions

Kornelius Tetzner: Conceptualization (lead); Formal analysis (lead); Funding acquisition (supporting); Investigation (lead); Methodology (lead); Project administration (lead); Writing-original-draft (lead); Writing-review-editing (lead). **Robert Schewski:** Formal analysis (lead); Writing-original-draft (supporting). **Andreas Popp:** Resources (lead); Writing-original-draft (supporting). **Saud Bin Anooz:** Investigation (supporting); Resources (supporting). **Ta-Shun Chou:** Investigation (supporting); Resources (supporting). **Ina Ostermay:** Methodology (equal). **Holm Kirmse:** Investigation (supporting); Resources (supporting); Validation (supporting); Writing – original draft (supporting); Writing – review & editing (supporting). **Joachim Würfl:** Conceptualization (supporting); Funding acquisition (lead); Investigation (supporting); Methodology (supporting); Project administration (supporting); Supervision (supporting); Writing-original-draft (supporting).

DATA AVAILABILITY

The data that support the findings of this study are available from the corresponding author upon reasonable request.

REFERENCES

[1] C. Wang, J. Zhang, S. Xu, C. Zhang, Q. Feng, Y. Zhang, J. Ning, S. Zhao, H. Zhou, and Y. Hao, J. Phys. D: Appl. Phys. **54**, 243001 (2021).
[2] H. Zhang, L. Yuan, X. Tang, J. Hu, J. Sun, Y. Zhang, Y. Zhang, and R. Jia, IEEE Trans. Power Electron. **35**, 5157 (2020).
[3] K. D. Chabak, K. D. Leedy, A. J. Green, S. Mou, A. T. Neal, T. Asel, E. R. Heller, N. S. Hendricks, K. Liddy, A. Crespo, N. C. Miller, M. T. Lindquist, N. A. Moser, R. C. Fitch, D. E. Walker, D. L. Dorsey, and G. H. Jessen, Semicond. Sci. Technol. **35**, 013002 (2020).
[4] S. J. Pearton, J. Yang, P. H. Cary, F. Ren, J. Kim, M. J. Tadjer, and M. A. Mastro, Appl. Phys. Rev. **5**, 011301 (2018).
[5] M. Higashiwaki and G. H. Jessen, Appl. Phys. Lett. **112**, 060401 (2018).
[6] Z. Hu, H. Zhou, Q. Feng, J. Zhang, C. Zhang, K. Dang, Y. Cai, Z. Feng, Y. Gao, X. Kang, and Y. Hao, IEEE Electron Device Lett. **39**, 1564 (2018).
[7] N. Allen, M. Xiao, X. Yan, K. Sasaki, M. J. Tadjer, J. Ma, R. Zhang, H. Wang, and Y. Zhang, IEEE Electron Device Lett. **40**, 1399 (2019).
[8] H. Zhou, Q. Feng, J. Ning, C. Zhang, P. Ma, Y. Hao, Q. Yan, J. Zhang, Y. Lv, Z. Liu, Y. Zhang, K. Dang, P. Dong, and Z. Feng, IEEE Electron Device Lett. **40**, 1788 (2019).
[9] Y. Lv, H. Liu, X. Zhou, Y. Wang, X. Song, Y. Cai, Q. Yan, C. Wang, S. Liang, J. Zhang, Z. Feng, H. Zhou, S. Cai, and Y. Hao, IEEE Electron Device Lett. **41**, 537 (2020).
[10] K. Tetzner, E. Bahat Treidel, O. Hilt, A. Popp, S. Bin Anooz, G. Wagner, A. Thies, K. Ickert, H. Gargouri, and J. Wurfl, IEEE Electron Device Lett. **40**, 1503 (2019).
[11] Z. Feng, Y. Cai, Z. Li, Z. Hu, Y. Zhang, X. Lu, X. Kang, J. Ning, C. Zhang, Q. Feng, J. Zhang, H. Zhou, and Y. Hao, Appl. Phys. Lett. **116**, 243503 (2020).
[12] N. K. Kalarickal, Z. Feng, A. F. M. Anhar Uddin Bhuiyan, Z. Xia, W. Moore, J. F. McGlone, A. R. Arehart, S. A. Ringel, H. Zhao, and S. Rajan, IEEE Trans. Electron Devices **68**, 29 (2021).
[13] C. Wang, H. Gong, W. Lei, Y. Cai, Z. Hu, S. Xu, Z. Liu, Q. Feng, H. Zhou, J. Ye, J. Zhang, R. Zhang, and Y. Hao, IEEE Electron Device Lett. **42**, 485 (2021).
[14] N. K. Kalarickal, Z. Xia, H.-L. Huang, W. Moore, Y. Liu, M. Brenner, J. Hwang, and S. Rajan, IEEE Electron Device Lett. **42**, 899 (2021).
[15] S. Sharma, K. Zeng, S. Saha, and U. Singisetti, IEEE Electron Device Lett. **41**, 836 (2020).
[16] P. R. Chalker, Thin Solid Films **343-344**, 616 (1999).
[17] P. G. Neudeck, R. S. Okojie, and L.-Y. Chen, Proc. IEEE **90**, 1065 (2002).
[18] M. A. Mastro, A. Kuramata, J. Calkins, J. Kim, F. Ren, and S. J. Pearton, ECS J. Solid State Sci. Technol. **6**, P356 (2017).
[19] Y. Yao, R. F. Davis, and L. M. Porter, J. Electron. Mater. **46**, 2053 (2017).
[20] Y.-W. Huan, S.-M. Sun, C.-J. Gu, W.-J. Liu, S.-J. Ding, H.-Y. Yu, C.-T. Xia, and D. W. Zhang, Nanoscale Res. Lett. **13**, 246 (2018).
[21] Y. Yao, R. Gangireddy, J. Kim, K. K. Das, R. F. Davis, and L. M. Porter, J. Vac. Sci. Technol., B **35**, 03D113 (2017).
[22] C. Fares, F. Ren, and S. J. Pearton, ECS J. Solid State Sci. Technol. **8**, Q3007 (2019).
[23] S. Bin Anooz, R. Grüneberg, C. Wouters, R. Schewski, M. Albrecht, A. Fiedler, K. Irmscher, Z. Galazka, W. Miller, G. Wagner, J. Schwarzkopf, and A. Popp, Appl. Phys. Lett. **116**, 182106 (2020).
[24] S. Bin Anooz, R. Grüneberg, T.-S. Chou, A. Fiedler, K. Irmscher, C. Wouters, R. Schewski, M. Albrecht, Z. Galazka, W. Miller, J. Schwarzkopf, and A. Popp, J. Phys. D: Appl. Phys. **54**, 034003 (2021).
[25] Z. Galazka, Semicond. Sci. Technol. **33**, 113001 (2018).
[26] Z. Galazka, R. Uecker, D. Klimm, K. Irmscher, M. Naumann, M. Pietsch, A. Kwasniewski, R. Bertram, S. Ganschow, and M. Bickermann, ECS J. Solid State Sci. Technol. **6**, Q3007 (2017).
[27] Z. Galazka, S. Ganschow, A. Fiedler, R. Bertram, D. Klimm, K. Irmscher, R. Schewski, M. Pietsch, M. Albrecht, and M. Bickermann, J. Cryst. Growth **486**, 82 (2018).
[28] M. Higashiwaki, K. Sasaki, A. Kuramata, T. Masui, and S. Yamakoshi, Appl. Phys. Lett. **100**, 013504 (2012).
[29] H. Zhou, M. Si, S. Alghamdi, G. Qiu, L. Yang, and P. D. Ye, IEEE Electron Device Lett. **38**, 103 (2017).
[30] C. Wang, H. Zhou, J. Zhang, W. Mu, J. Wei, Z. Jia, X. Zheng, X. Luo, X. Tao, and Y. Hao, Appl. Phys. Lett. **120**, 112101 (2022).
[31] K. Sasaki, M. Higashiwaki, A. Kuramata, T. Masui, and S. Yamakoshi, Appl. Phys. Express **6**, 086502 (2013).
[32] Z. Xia, C. Joishi, S. Krishnamoorthy, S. Bajaj, Y. Zhang, M. Brenner, S. Lodha, and S. Rajan, IEEE Electron Device Lett. **39**, 568 (2018).
[33] M.-H. Lee and R. L. Peterson, ECS J. Solid State Sci. Technol. **8**, Q3176 (2019).
[34] M.-H. Lee and R. L. Peterson, APL Mater. **7**, 022524 (2019).
[35] M. Hirose, T. Nabatame, K. Yuge, E. Maeda, A. Ohi, N. Ikeda, Y. Irokawa, H. Iwai, H. Yasufuku, S. Kawada, M. Takahashi, K. Ito, Y. Koide, and H. Kiyono, Microelectron. Eng. **216**, 111040 (2019).
[36] A. Bhattacharyya, S. Roy, P. Ranga, D. Shoemaker, Y. Song, J. Spencer Lundh, S. Choi, and S. Krishnamoorthy, Appl. Phys. Express **14**, 076502 (2021).